Journal of Superconductivity and Novel Magnetism (2018) 31:3841–3845
https://doi.org/10.1007/s10948-018-4676-x

ORIGINAL PAPER

# Magnetic Properties and Critical Current of Superconducting Nanocomposites $(1-x)YBa_2Cu_3O_{7-\delta} + xCuO$

A. A. Lepeshev[1,2] · G. S. Patrin[2,3] · G. Yu. Yurkin[2,3] · A. D. Vasiliev[2,3] · I. V. Nemtsev[3] · D. M. Gokhfeld[2,3] · A. D. Balaev[3] · V. G. Demin[1,2] · E. P. Bachurina[1,2] · I. V. Karpov[1,2] · A. V. Ushakov[1,2] · L. Yu. Fedorov[1,2] · L. A. Irtyugo[2] · M. I. Petrov[1,3]

Received: 14 March 2018 / Accepted: 29 March 2018 / Published online: 11 April 2018


**Abstract**
The aim of this paper was to study the effect of nanoscale inclusions of CuO as the second ingredient of composites on transport properties of superconducting $YBa_2Cu_3O_7$ polycrystals. The samples of $YBa_2Cu_3O_{7-\delta}$ with different content of CuO nanoparticles were synthesized. The analysis of the magnetic properties was carried out within the extended critical state model. It was found that the addition of 0.5 and 1% of CuO nanoparticles leads to an increase in the intragranular density of the critical current at $T = 4.2$ K. A further increase of $x$ from 2 to 15% and more than 40% decreases the critical current density. The critical current density higher than in the reference sample was also found in the samples with $x = 20\%$ and $x = 24\%$.

**Keywords** Superconducting polycrystals · YBCO ceramics · Critical current · Magnetic properties

## 1 Introduction

Nowadays, increasing the critical current density in superconductors is achieved by various methods [1]. A large number of studies devoted to this problem were caused by its practical importance. The improvement of current-carrying properties of a superconductor occurs during the creation of structural defects in the material. These defects act as the pinning centers of Abrikosov vortices. The creation of pinning centers in high-temperature superconductors (HTSCs) as well as their thermal and chemical stability has been described in the literature in detail [1–4]. The most well-known methods for creating structural defects turn out to be the radiation exposure [1], the introduction of various cations into the crystal lattice [2, 3], and the introduction of nonsuperconducting particles into the superconductor [1, 4]. These methods have two disadvantages: firstly, radiation defects are nondurable; secondly, foreign impurities inside the superconductor often reduce the critical temperature. Surface decoration [6–8] is a new method, in which pinning centers are created only on the surface of a sample or superconducting granules. Nanoparticles of metal oxides can act as decorating elements.

While studying the transport properties of HTSC + CuO composites, it was found that the chemical interaction of $YBa_2Cu_3O_{7-\delta}$ with CuO is negligible [3–5] unlike the ferrite compositions [6, 7]. With the appearance of the technology for creating nanoscale CuO particles, it seems logical to study the effect of nanoscale inclusions of CuO as the second ingredient of composites on transport properties of superconducting $YBa_2Cu_3O_7$ polycrystals, which is the focus of this studies.

## 2 Experimental

Composites with different contents of CuO nanoparticles were synthesized with the ceramic technology. $YBa_2Cu_3O_{7-\delta}$ was synthesized from CuO, $BaCO_3$, and $Y_2O_3$ at the temperatures of up to 930 °C with intermediate grinding (up to ten times).

✉ A. A. Lepeshev
sfu-unesco@mail.ru

1 Federal Research Center Krasnoyarsk Scientific Center of the Siberian Branch of the Russian Academy of Science, Krasnoyarsk, 660036, Russia

2 Siberian Federal University, Krasnoyarsk, 660041, Russia

3 Kirensky Institute of Physics, Federal Research Center KSC SB RAS, Krasnoyarsk, 660036, Russia

The synthesis of CuO nanopowder was performed in a plasma-chemical reactor, described in [8–12]. The arc evaporator, used in the process, had the following characteristics: a current arc of 100 A and an intensity of the longitudinal magnetic field excited by a focusing coil on the surface of the cathode, of 80 A/m, with a distance between the cathode and the anode of $d = 50$ mm. A rod, made of high-purity copper (99.99%) with a diameter of 80 mm and a length of 100 mm, was used as a sputtering cathode. It was placed on a water-cooled copper current lead. In order to begin plasma chemical reactions, the chamber gas was preliminary pumped out to a pressure of $p = 1$ mPa and then it was filled by a gas mixture containing 40 vol% $O_2$ from $N_2$ plasma-generating gas in the input. To study the pressure influence, nanoparticles were synthesized at a basic pressure of 80 Pa. Oxygen was supplied to the reactor in order to form a uniform layer around the plasma torch. The reaction products were collected within 10 min on a hemispherical collector made of water-cooled stainless steel, placed at a distance of 0.12 m from the cathode. Table 1 describes the operating parameters of the reactor which were set before the synthesis.

The morphological composition of the samples was studied by transmission electron microscope JEOL JEM-2100. Studying the phase composition of the samples was carried out using an Advance D8 X-ray diffractometer in CuK$\alpha$ monochromatic radiation. Scanning was performed at room temperature in the range of angles at 30–70° with $2\theta$ step of 0.06°.

First, composites with different volumetric contents of CuO were annealed at 900 °C for 1 h and then moved to the furnace under a temperature of 400 °C where they were held for 24 h. To calculate the volumetric percentage of the composites' ingredients, we used the following densities: CuO $\rho = 5.805$ g/cm$^3$ and $YBa_2Cu_3O_{7-\delta}\rho = 6.36$ g/cm$^3$. In sintered samples, one side was ground for X-ray-structure measurements. Magnetic measurements were carried out with the MPMS-XL5 unit. Debye X-ray patterns were recorded on a diffractometer D8 ADVANCE (Bruker AXS).

Measurements of the isothermal dependences of the magnetization on the magnetic field were carried out at temperatures of 4.2 and 77 K. The critical current density of the samples was estimated by a magnetic hysteresis loop using an extended critical state model [13, 14].

**Table 1** Operating parameters of a vacuum plasma-chemical reactor for CuO synthesis

| Parameter | Conditions |
|---|---|
| Basic pressure in chamber | $10^{-3}$ Pa |
| Arc discharge current | 100 A |
| Voltage | 70 V |
| Power | 10 kW |
| Supply of plasma-forming gas (nitrogen) | 60 Pa |
| Supply of reaction gas (oxygen) | 40 vol% $O_2$ |

## 3 Results and Analysis

Figure 1 shows the TEM image, histogram, and probability density functions of nanosized copper oxide nanoparticles produced at the pressure of the gas mixture (40 vol% $O_2$ + 60% $N_2$) of 80 Pa.

It is obvious from the results above that the produced powder represents strongly agglomerated particles of a spherical shape. The particle size ranges from 5 to 20 nm. The combination of normal and log-normal size distributions characterizes these particles. This suggests two competing mechanisms of particle condensation from a steam-plasma phase: cluster and steam condensations. The mixed density function under study represents the sum of the density functions of lognormal and normal distributions with adjustable parameters. It is obvious from the figure above that this function describes the particle size distribution much better. The average particle size was 12.4 nm, the mean mass particle size was 13.2 nm, and the standard deviation was 1.18.

Nanopowders are characterized by a high surface energy, which is compensated by a significant aggregation of powders, and this process causes a significant decrease of the specific surface. Since the nanoparticle synthesis in a plasmachemical reactor is always accompanied by definite chemical processes, the size distribution function of nanoparticles becomes more complicated because of the products of these reactions. The morphology of the particles also becomes more complicated, and various particles of different chemical composition are formed. Besides, interdiffusion of nanoparticles in the condensed phase occurs.

Under a sufficiently high temperature, multiple processes can occur simultaneously, forming strong coupling between the nanoparticles. The experimental data are described by a normal distribution while prevailing nanoparticles layered growth due to the adsorption of atoms and the diffusion processes during corresponding atomic mass transfer at the interface.

Figure 2 shows the X-ray diffraction pattern of nanoparticles, synthesized under the pressure of the gas mixture (40 vol% $O_2$ + 60% $N_2$) for the values of $2\theta$ in the range from 30 to 70°.

The XRD pattern clearly illustrates that the copper oxide nanoparticles, formed during the synthesis, have a crystalline nature, and the monoclinic crystal structure of CuO (PDF 4+ #00-045-0937) with lattice parameters of $a = 4.691$ Å, $b = 3.432$ Å, and $c = 5.138$ Å.

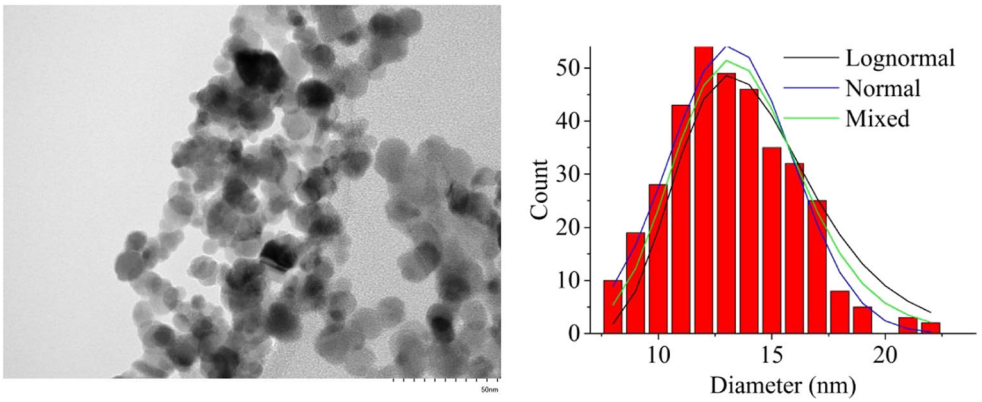


**Fig. 1** TEM image, histogram, and probability density functions of nanosized copper oxide powders produced under the pressure of the gas mixture (40 vol% $O_2$ + 60% $N_2$) equal to 80 Pa

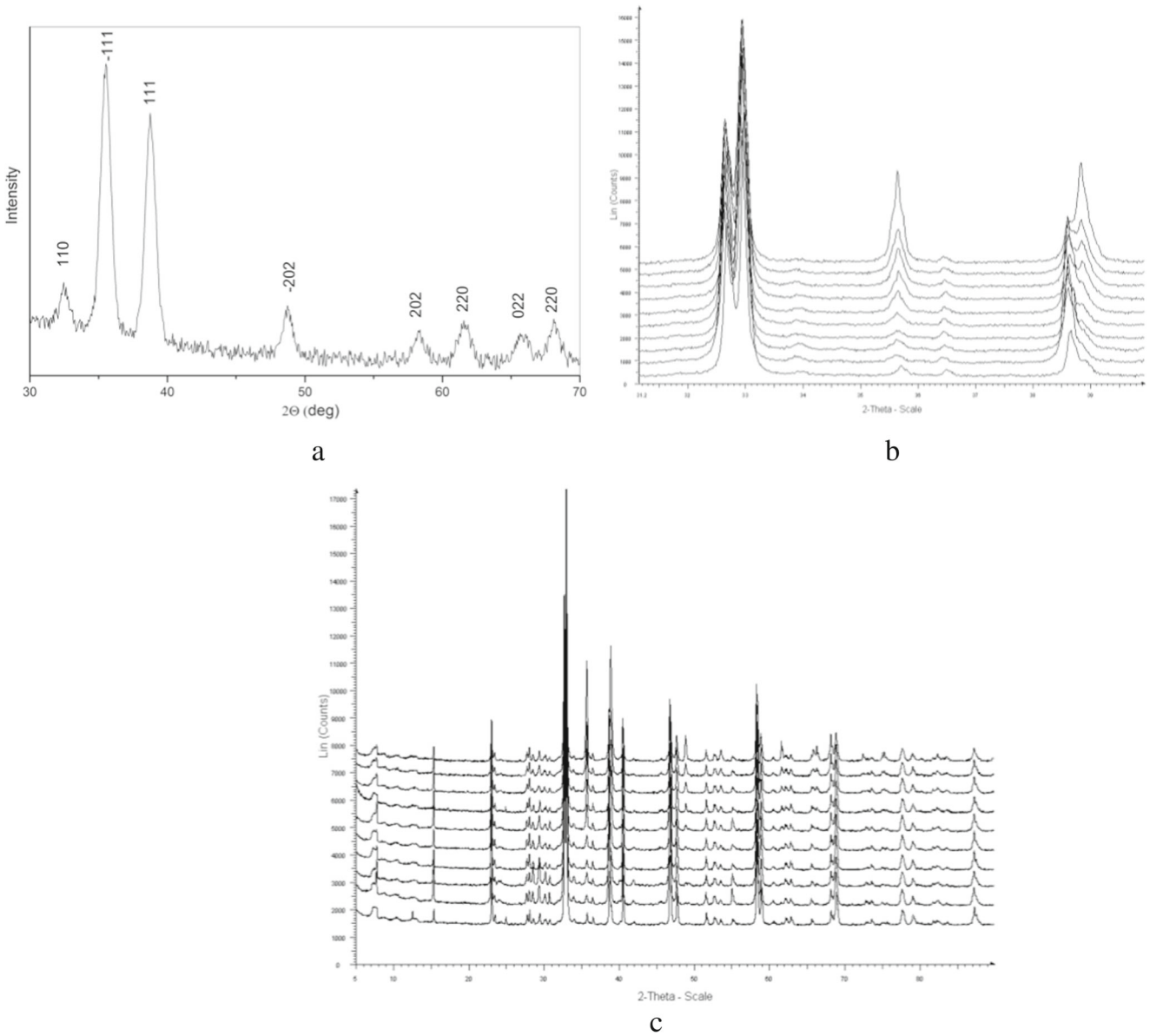


**Fig. 2** XRD pattern of **a** CuO nanopowder produced under the pressure of the gas mixture (40 vol% $O_2$ + 60% $N_2$) equal to 80 Pa; **b** CuO in composite; **c** composite sample

The Debye X-ray pattern of nanoscale CuO is typical for nanocrystals, i.e., the reflections are shifted and significantly broadened. In composites, the parameters of the reflexes from CuO return to the appearance which is characteristic of massive crystallites. Thus, the temperature conditions of annealing the composites lead to a partial recrystallization of the copper oxide. The Debye X-ray patterns of composites represent a superposition of reflections from CuO and $YBa_2Cu_3O_{7-\delta}$ structures. Additional reflexes were not observed in the experiment, which indicated the absence of a chemical interaction of CuO with the $YBa_2Cu_3O_{7-\delta}$ superconductor. Figure 2c shows fragments of the Debye X-ray patterns of composite samples in the region of $2\theta$ from 31.2 to 40° in which a monotonic increase in the intensities of the reflections is observed at $2\theta = 35.559°$ (−1 −1 1) and at $2\theta = 38.754°$ (111) with increasing CuO content.

The hysteresis loops of the magnetization of the samples are shown in Fig. 3. Figure 3 shows the dependences of the nonequilibrium magnetization $\Delta M(H)$ obtained from the measurement of the hysteresis width along the $M$ axis. Samples with $x = 0.5$, 1, and 2% have larger values of $\Delta M$ than the sample with $x = 0$, where $x$ is a content of CuO nanoparticles. Samples with $x = 20$ and 24% have $\Delta M$ values that are slightly lower than the sample with $x = 0$. For other samples, the values of $\Delta M$ are much lower.

The total magnetization of the investigated samples $M(H)$ also contains the equilibrium magnetic contribution $M_N(H)$, which increases with an increasing CuO content. The hysteresis loop of superconducting granule magnetization is defined as $M_S(H) = M(H) - M_N(H)$. For all the samples, the line section of the initial magnetization from $H = 0$ to $H = H_{c1}$ of the $M_S(H)$ dependencies has the same slope, which indicates the same density of superconducting granules.

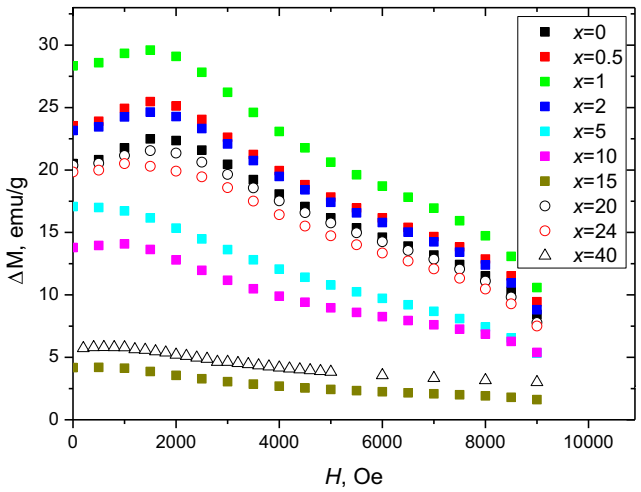


**Fig. 3** Nonequilibrium magnetization of the samples at $T = 4.2$ K

The critical current density $J_c$ was determined according to the equation

$$J_c = 3\Delta M_S/2R \quad (1)$$

where $\Delta M_S$ is the nonequilibrium magnetization of superconducting granules, $\Delta M_S = \Delta M * 100/(100 - x)$, and $R$ is the current circulation radius.

The value of $R$ depends on the magnetic field. In small fields (less than 100 Oe), $R$ is equal to the radius of the sample [15]. In high fields, the superconductivity of the intergranular boundaries is completely suppressed by the magnetic field, and the magnetic properties of the polycrystalline sample can be determined only by the magnetization of the granules. Thus, for $H > 100$ Oe, the value of $R$ is equal to the average radius of the granules. Equation (1) allows calculating the intragranular density of the critical current for the loops of magnetization, measured up to large fields.

The average radius of the granules, $R \sim 2\mu$m, was determined from the micrographs of the samples. The extended critical state model allows obtaining more accurate estimates of $R$ from the asymmetry of the magnetization loop with respect to the $H$ axis. The measured magnetization loops of different samples have different asymmetries. The asymmetry of the magnetization loop is determined by the ratio of the penetration depth of the magnetic field λ to the radius of the granule. From the extended critical state model, it can be concluded that $J_c = j_c(1 - l/R)^3$, where $j_c$ is the critical current density of the sample with $R >> \lambda$. To the sample with $R >> \lambda$, the following equality is applied: $\Delta M_S = 2M_{upS}$, where $M_{upS}$ is the branch of the magnetization loop of superconducting granules in the increasing field. Thus, the equation should look the following way:

$$l/R = 1 - (\Delta M_S/2M_{upS})^{1/3} \quad (2)$$

Given $l = \lambda = 200$ nm for YBCO, this equation was used to determine $R$. The values of $\Delta M_S$ and $M_{upS}$ were measured in the field $H_p \sim 5000$ Oe. The value of $H$ is approximately equal to value of the field of complete penetration of the magnetic flux into the granules at the given temperature. For $H < H_p$, the expression of the critical state model for $J_c$ determination gives underestimated values [14, 15]. The estimation of the circulation radii shows that the average size of the granules increases from $R = 1.9$ $\mu$m in the sample with $x = 0$ to $R = 2.7$ $\mu$m in the sample with $x = 10\%$. With further growth of $x$, values of $R$ decrease up to 2.1–2.2 $\mu$m in the samples with $x \geq 20\%$. The dependences $J_c(H)$ shown in Fig. 4 were determined from the magnetization loops $M_S(H)$ according to Eq. (1) of the critical state model using the obtained values of $R$. Figure 4 shows the values of $J_c$ in the field of 2000 Oe (near the field of total penetration at this temperature). An increase in $J_c$ is observed for the samples with $x = 0.5\%$ and $x = 1\%$,

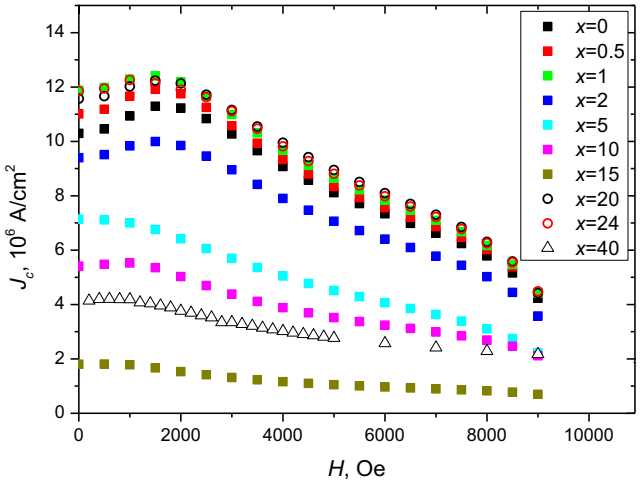


**Fig. 4** The dependence of the density of the intragranular critical current on the magnetic field at $T = 4.2$ K

as well as for the samples with$x = 20\%$ and $x = 24\%$ in comparison with $x = 0$.

At the temperature of 77 K, the dependence of the parameters on $x$ changes. For any value of $H$, the irreversible magnetization $\Delta M_S$ decreases when $x$ increases. However, the density of the intragranular critical current decreases (with increasing $x$) only in the range from 0 to 15%. With further increase in$x$, $J_c$ increases, achieving the maximum at $x = 40\%$. Figure 5 shows the values of $J_c$ in the field of 200 Oe (near the field of total penetration at this temperature).

We assume that at low temperatures the increase in the critical current is due to pinning on single particles with dimensions of tens of nanometers on the surface of the granules. If the temperature increases, the pinning contribution to such small surface particles decreases because of the increase in the coherence length. At 77 K, the pinning mainly occurs on larger particles located on the surface of the HTSC

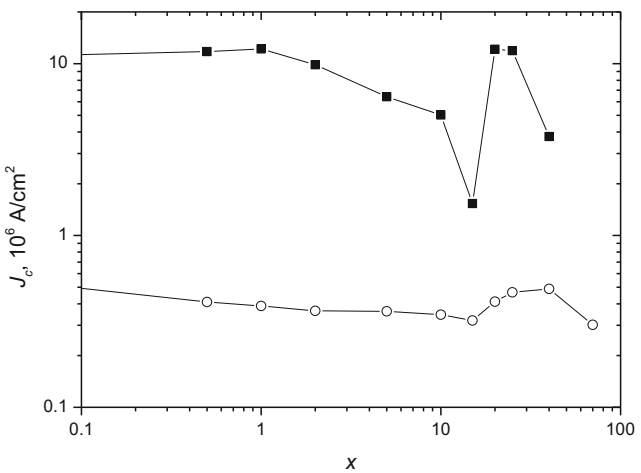


**Fig. 5** The dependence of critical current density on the volume content of CuO nanoparticles at $T = 4.2$ K, $H = 2000$ Oe (filled squares), and at $T = 77$ K, $H = 200$ Oe (empty circ)

granules. In fact, an increase in the pinning force is observed at high CuO concentrations. These concentrations, according to XRD, cause the increase in the number of larger particles. Accordingly, the enhancement of pinning at high temperatures occurs at concentrations near the percolation threshold, which for random systems is equal to 0.238.

## 4 Conclusion

The microstructure and magnetic properties of the YBaCuO superconductor with different contents of CuO nanoparticles have been studied. It has been established that the addition of nanosized CuO particles leads to the increase in the density of the intragranular critical current at $T = 4.2$ K for the concentrations of $x = 0.5$, 1, 20, and 24% and at $T = 77$ K for the concentrations of $x = 20$, 24, and 40%. Such an increase in the critical current is due to CuO nanoparticles which appear on the surface of superconducting granules. These granules become effective pinning centers for Abrikosov vortices. With a temperature increase, efficient pinning occurs on CuO particles of a larger size.

**Acknowledgments** The work was performed with a support of the grant of the Russian Science Foundation (project no. 16-19-10054).

## References

1. Kazin, P.E., Tretyakov, Yu.D.: Chemical Success **72**, 10 (2003)
2. Altin, E., Gokhfeld, D.M., Komogortsev, S.V., Altin, S., Yakinci, M.E.: J. Mater. Sci.: Mater. Electron. **24**, 1341 (2013)
3. Petrov, M.I., Balaev, D.A., Shaykhutdinov, K.A., Aleksandrov, K.S.: Phys. Solid State **41**, 881 (2002)
4. Petrov, M.I., Gokhfeld, Yu.S., Balaev, D.A., Popkov, S.I., Dubrovskiy, A.A., Gokhfeld, D.M., Shaykhutdinov, K.A.: Supercond. Sci. Technol. **21**, 085015 (2008)
5. Balaev, A.D., Gohfeld, D.M., Popkov, S.I., Shaikhutdinov, K.A., Petrov, M.I.: Tech. Phys. Lett. **27**, 952 (2001)
6. Lepeshev, A.A., Karpov, I.V., Ushakov, A.V., Nagibin, G.E.: J Alloys Compounds **663**, 631 (2016)
7. Lepeshev, A.A., Ushakov, A.V., Karpov, I.V.: J. Appl. Phys. **122**, 104103 (2017)
8. Ushakov, A.V., Karpov, I.V., Lepeshev, A.A., Fedorov, L.Yu.: Int. J. Nanosci. **16**, 1750001 (2017)
9. Ushakov, A.V., Karpov, I.V., Lepeshev, A.A., Petrov, M.I.: J. Appl. Phys. **118**, 023907 (2015)
10. Ushakov, A.V., Karpov, I.V., Lepeshev, A.A., Petorv, M.I., Fedorov, L.Yu.: JETP Letters. **99**, 99 (2014)
11. Karpov, I.V., Ushakov, A.V., Lepeshev, A.A., Fedorov, L.Yu.: Tech. Phys. **62**, 168 (2017)
12. Karpov, I.V., Ushakov, A.V., Fedorov, L.Y.u., Lepeshev, A.A.: Tech. Phys. **84**, 559 (2014)
13. Gokhfeld, D.M., Balaev, D.A., Petrov, M.I., Popkov, S.I., Shaykhutdinov, K.A., Valkov, V.V.: J. Appl. Phys. **109**, 033904 (2011)
14. Gokhfeld, D.M.: Phys. Solid State **56**, 2380 (2014)
15. Landau, I.L., Willems, J.B., Hulliger, J., Phys, J.: Condens. Matter **20**, 095222 (2008)